

High Efficiency Wide Input Voltage Range LCLC Resonant Converter Using Nonlinear Frequency Controller

Bo Sheng, Yang Chen, Hongliang Wang, Yan-Fei Liu, *Fellow, IEEE*, Paresh C. Sen, *Life Fellow IEEE*

Department of Electrical and Computer Engineering
Queen's University,
Kingston, Canada
bo.sheng@queensu.ca, yanfei.liu@queensu.ca

Abstract— In server and telecommunication applications, LLC resonant converter featuring high efficiency and high power density becomes an excellent candidate for the front-end DC/DC stage. But, for conventional LLC converter, the performance will be severely deteriorated once the converter is designed for accommodating regulation over wide input voltage range. A modified LLC topology with changeable magnetizing inductance, LCLC resonant converter, has been successfully proved to extend the input voltage range without sacrificing the normal efficiency. Moreover, due to the strong nonlinear feature of the LCLC resonant converter, conventional linear control strategies such as PI controller are very hard to optimize. This paper proposes a nonlinear frequency control method for LCLC converter to achieve better output voltage regulation over wide input voltage range. In the controller, the switching frequency is calculated from a quadratic function, which expresses the opposite variation of the voltage gain. Finally, a 250 – 400V input 12V/500W output LCLC prototype is built and tested. Experimental results demonstrate the effectiveness of the proposed nonlinear frequency control strategy.

Keywords – resonant converter, LCLC, wide input voltage range, nonlinear frequency controller

I. INTRODUCTION

Recently, the consumer desire of smaller, lighter and more efficient electronics has led to the development of the power supplies [1, 2]. Resonant converters are receiving more and more attention owing to their features of higher efficiency and higher power density when compared to conventional pulse width modulation (PWM) converters [3, 4]. Of all resonant converters, LLC resonant converter is widely used as the front-end DC/DC converter due to its ability of achieving zero voltage switching (ZVS) for primary side switches over entire operating range and zero current switching (ZCS) for secondary side rectifiers when operates below the resonance.

To meet the hold-up time requirement, DC/DC converters in server and telecommunication applications are preferred to be designed with wide input voltage range. Otherwise, a large electrolytic capacitor will be added on DC bus, which will defeat the purpose of improving the power density [5]. However, it is well-known that the LLC resonant

converter is not suitable for wide input voltage range. This is because a small magnetizing inductance is needed to achieve high voltage gain when input voltage goes low. Such design increases the RMS current and the turn-off current of the primary side switches, causing high conduction loss and turn-off loss.

To solve this problem, several modifications based on LLC topology were proposed, including cascading a baby boost converter to narrow the DC bus voltage range [6], adding another resonant branch to double the voltage gain at low input voltage [7], or utilizing auxiliary windings on secondary side to increase the voltage gain [8]. Although these methods could extend the input voltage range of the LLC converter, they add lots of extra components and making the configuration complex. One another proposal was to drive the half bridge switches with asymmetric pulse width modulation (APWM) instead of pulse frequency modulation (PFM) [9]. However, this proposal not only limits the peak gain enhancement, but complicates the control strategy. LCLC resonant converter has been seen to extend input voltage range while maintaining excellent efficiency [10]. A capacitor is added in series with the magnetizing inductor to form the LCLC resonant converter, as shown in Fig. 1. The equivalent parallel impedance keeps inductive under normal operating conditions. Therefore, the resonant tank is actually an L-L-C structure featuring changeable magnetizing inductance. The PFM method could also be used to regulate the output voltage, leading to an easy-to-control resonant converter with high reliability.

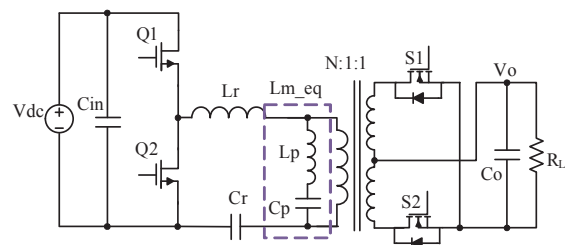


Fig. 1. Structure of the LCLC resonant converter

Because of the strong nonlinear feature of the LCLC resonant converter, the output voltage regulation is more difficult than conventional PWM-based converter. Conventional linear controllers such as PI controller are often applied to obtain expected voltage regulation performance, but they are only valid in the small vicinity of a specific operation point. In [11], two sets of PI parameters were used to regulate the output voltage at light load and heavy load. This method could improve the voltage regulation performance, but it still faces the problem of linear methods. In [12], a feedback linearization control strategy is proposed. However, the feasibility over wide input voltage range is not considered.

In this paper, a nonlinear frequency control strategy is proposed to achieve better output voltage regulation over wide input voltage range. Moreover, the proposed method could improve the transient response at high input voltage. A microcontroller is used to calculate the desired switching frequency for primary side switches. Due to the limited sensing and calculation work, a low-cost MCU is chosen in practice. Simulation and experimental results are given to verify the proposed control strategy.

II. DESIGN OF THE FEEDBACK COMPENSATOR

From Fig. 1, the equivalent magnetizing inductor L_{m_eq} is consisted by a parallel inductor L_p and a parallel capacitor C_p connected in series. The L_{m_eq} is changing along with the switching frequency and can be calculated in (1).

$$L_{m_eq} = L_p - \frac{1}{(2\pi f_{sw})^2 C_p} \quad (1)$$

Where, f_{sw} is the switching frequency. With high input voltage, the L_{m_eq} is of a large value as switching frequency is high. In this way, the primary side RMS current is reduced. With low input voltage, the L_{m_eq} is decreased because of the reduction of switching frequency, thus, high voltage gain can be achieved.

By ignoring all higher order harmonics, the LCLC resonant converter can be simplified as a first order sinusoidal circuit, as shown in Fig. 2. Then, the relationship between input and output voltage is calculated in (2).

$$M_g = \frac{V_{oe}}{V_{ge}} = \frac{1}{\sqrt{\left(1 + \frac{1}{L_{n_eq}} - \frac{1}{L_{n_eq} f_n^2}\right)^2 + Q_e^2 \left(f_n - \frac{1}{f_n}\right)^2}} \quad (2)$$

Where,

$$f_n = \frac{f_{sw}}{f_r}$$

$$L_{n_eq} = \frac{L_{m_eq}}{L_r}$$

$$Q_e = \frac{\sqrt{L_r / C_r}}{R_e}$$

$$R_e = \frac{8N^2 / \pi^2}{R_o}$$

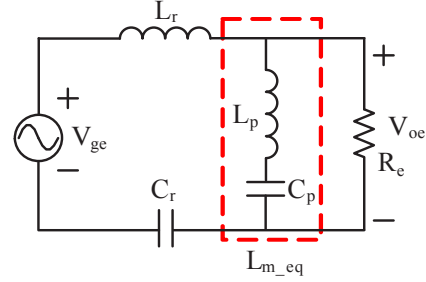


Fig. 2. Sinusoidal model of the LCLC resonant converter

Fig. 3 compares the voltage conversion ratio of the LCLC converter with parallel capacitor C_p and the LLC converter without C_p . The specifications of the converters are shown in Table. I. From Fig. 3, the LCLC resonant converter has a much steeper voltage gain curve, implying that within the same switching frequency range, it is easier to realize wider input voltage operation than conventional LLC resonant converter.

TABLE I. SPECIFICATIONS OF DESIGNED LCLC CONVERTER

V_{in}	250 – 400 VDC	L_r	11 μ H
V_{out}	12 VDC	L_p	227 μ H
P_{out}/I_{out}	500 W/42 A	C_r	20 nF
N	17	C_p	5 nF
f_{min}	170 kHz	f_{max}	260 kHz

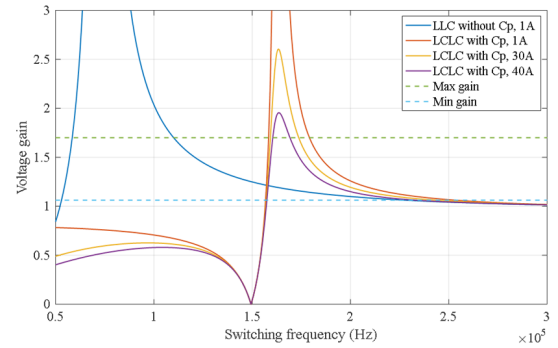


Fig. 3. Voltage conversion ratios of the LCLC converter with C_p and LLC converter without C_p

Unlike conventional PWM-based converter, the small signal model of LLC converter cannot be obtained from the state-space averaging method since its switching frequency is close to the natural frequency of the resonant tank [13]. Generally, extended describing function (EDF) method is applied to model the LLC resonant converter as this method considers all switching frequency harmonics for accuracy [14]. LCLC resonant converter, similar to conventional LLC resonant converter, can also be modeled by using the EDF

method. The state-space model of the LCLC resonant converter is shown in (3).

$$A = \begin{bmatrix} \frac{H_{ip} + r_s}{L_r} & \frac{\Omega_s L_s + H_{ic}}{L_r} & -\frac{1}{L_r} & 0 & \frac{H_{ip}}{L_r} & \frac{H_{ic}}{L_r} & -\frac{H_{vcf}}{L_r} \\ \frac{\Omega_s L_s - G_{ip}}{L_r} & \frac{G_{ic} + r_s}{L_r} & 0 & -\frac{1}{L_r} & \frac{G_{ip}}{L_r} & \frac{G_{ic}}{L_r} & -\frac{G_{vcf}}{L_r} \\ \frac{1}{C_r} & 0 & 0 & -\frac{\Omega_s C_r}{C_r} & 0 & 0 & 0 \\ 0 & \frac{1}{C_r} & \frac{\Omega_s C_r}{C_r} & 0 & 0 & 0 & 0 \\ \frac{H_{ip}}{L_{m-eq}} & \frac{H_{ic}}{L_{m-eq}} & 0 & 0 & -\frac{H_{ip}}{L_{m-eq}} & -\frac{H_{ic} + L_{m-eq}\Omega_s}{L_{m-eq}} & \frac{H_{vcf}}{L_{m-eq}} \\ \frac{G_{ip}}{L_{m-eq}} & \frac{G_{ic}}{L_{m-eq}} & 0 & 0 & -\frac{G_{ip} - L_{m-eq}\Omega_s}{L_{m-eq}} & -\frac{G_{ic}}{L_{m-eq}} & \frac{G_{vcf}}{L_{m-eq}} \\ \frac{K_{is}r_c'}{C_f r_c'} & \frac{K_{ic}r_c'}{C_f r_c'} & 0 & 0 & -\frac{K_{is}r_c'}{C_f r_c'} & -\frac{K_{ic}r_c'}{C_f r_c'} & -\frac{r_c'}{RC_f r_c'} \end{bmatrix}$$

$$B = \begin{pmatrix} -\frac{L_s \omega_o I_c}{L_s} & \frac{L_s \omega_o I_s}{L_s} & -\frac{C_s \omega_o V_c}{C_s} & \frac{C_s \omega_o V_s}{C_s} & -\frac{L_m \omega_o I_{mc}}{L_m} & \frac{L_m \omega_o I_{ms}}{L_m} & 0 \end{pmatrix}$$

$$C = \begin{pmatrix} K_{is}r_c' & K_{ic}r_c' & 0 & 0 & -K_{is}r_c' & -K_{ic}r_c' & \frac{r_c'}{r_c} \end{pmatrix}, D = 0$$

$$\frac{d\hat{x}}{dt} = A\hat{x} + B\hat{u}, \hat{y} = C\hat{x} + D\hat{u}$$

$$\frac{\hat{y}_o}{\hat{\omega}_{sn}} = C(SI - A)^{-1}B + D \quad (3)$$

Where, A , B , C , and D are the state-space system matrices, and $\hat{x} = (\hat{i}_s \ \hat{i}_c \ \hat{v}_s \ \hat{v}_c \ \hat{i}_{ms} \ \hat{i}_{mc} \ \hat{v}_{cf})$ is the state vector.

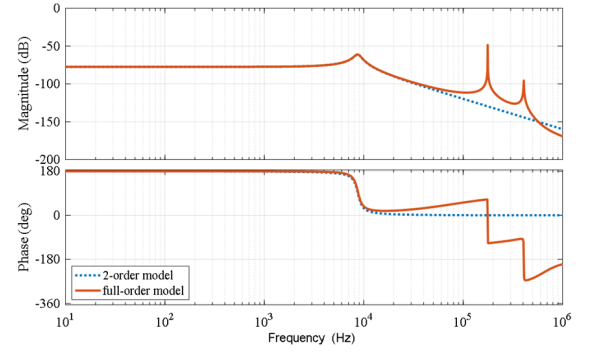
By neglecting the poles and zeros beyond the switching frequency, the transfer function of the LCLC converter can be simplified as (4).

$$G_p(s) = \frac{G_{po}(s + \omega_{esr})(s - \omega_{RHP})}{\left(s^2 + \frac{\omega_{p1}}{Q_1}s + \omega_{p1}^2\right)\left(s^2 + \frac{\omega_{p2}}{Q_2}s + \omega_{p2}^2\right)} \quad (4)$$

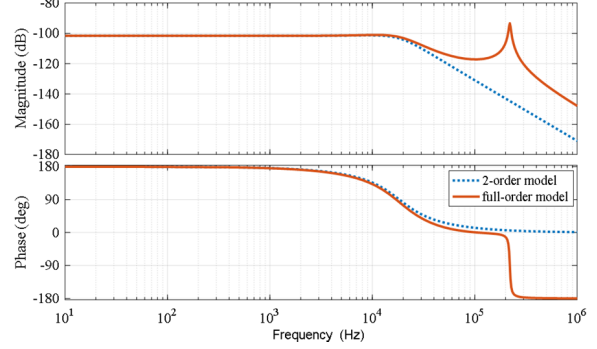
Only taking the dominant poles into consideration, the system can be further simplified as a 2-order model, shown in (5).

$$G_p(s) = -\frac{G_{po}\omega_{esr}\omega_{RHP}}{\omega_{p2}^2} \frac{1}{s^2 + \frac{\omega_{p1}}{Q_1}s + \omega_{p1}^2} \quad (5)$$

To verify the accuracy of the simplified 2-order model, Fig. 4 presents the bode plots of the full order and the simplified 2-order models which are both built in MATLAB. The solid lines and dot lines represent the full order and simplified 2-order models, respectively. It can be seen from Fig. 4, two models share the similar frequency characteristics in the low and medium frequency range. But, in high frequency range, simplified 2-order model attenuates much quicker than full order model. This is because poles and zeros beyond the switching frequency are excluded. The simplified 2-order model is accurate enough for designing the compensator.



(a) 250V input and 1A output



(b) 400V input and 40A output

Fig. 4. Frequency response of the designed LCLC resonant converter

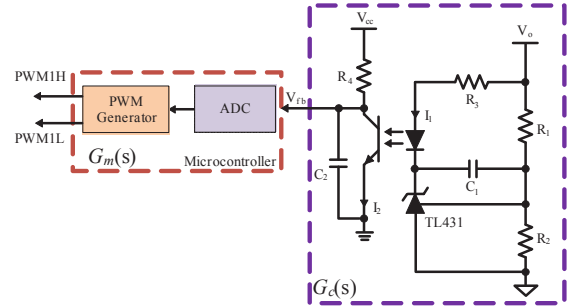


Fig. 5. Circuit diagram of the feedback controller

Fig. 5 shows the circuit diagram of the proposed controller. A typical “TL431 + optocoupler” circuit is used to implement output voltage regulation and provide electrical isolation between primary and secondary sides. A microcontroller first senses the feedback single V_{fb} by using ADC module, then, calculates the desired switching frequency based on the sensed V_{fb} , finally, outputs PWM signal to primary side switches. This controller varies the switching frequency to regulate the output voltage to be equal to $(1 + R_1/R_2) \times 2.5V$. The overall system's loop gain can be determined as shown in (6).

$$T_m(s) = G_p(s) \cdot G_c(s) \cdot G_m(s) \quad (6)$$

Where, $G_c(s)$ is the transfer function of the feedback compensator, and $G_m(s)$ is the gain of the PWM generator.

The transfer function of the feedback compensator is calculated in (7).

$$G_c(s) = \frac{V_{fb}}{V_o} = -CTR \frac{R_4}{R_3} \left(\frac{1 + sR_1C_1}{sR_1C_1(1 + sR_4C_2)} \right) \quad (7)$$

The resistor R_3 limits the current flowing through the optocoupler LED. The maximum current in the LED is expressed in (8).

$$I_{l-max} = \frac{V_o - V_{forward} - V_{TL431-min}}{R_3} \quad (8)$$

Where, $V_{forward}$ is the optocoupler LED forward voltage drop, and $V_{TL431-min}$ is the minimum cathode-to-anode voltage of the TL431. The current reflected to the optocoupler collector side is then derived in (9).

$$I_{2-max} = I_{l-max} CTR \quad (9)$$

Where, CTR is optocoupler's current transfer ratio. Then, the minimum feedback voltage can be determined in (10).

$$V_{fb-min} = V_{cc} - I_{2-max} R_4 \quad (10)$$

Besides, the maximum feedback voltage V_{fb-max} is equal to V_{cc} when there is no current flowing through the optocoupler collector side.

In the compensator, the microcontroller varies the switching frequency based on the sensed V_{fb} and works like a voltage-controlled oscillator (VCO). Typically, the relationship between the feedback voltage V_{fb} and the switching period T_{sw} is linear as shown in (11).

$$T_{sw} = (kV_{fb} + b) F_n \quad (11)$$

$$f_{sw} = \frac{1}{T_{sw}} = \frac{1}{kV_{fb} + b} \frac{1}{F_n}$$

Where, k and b are constant parameters, T_{sw} is the calculated switching period value, and F_n is the PWM resolution of the microcontroller.

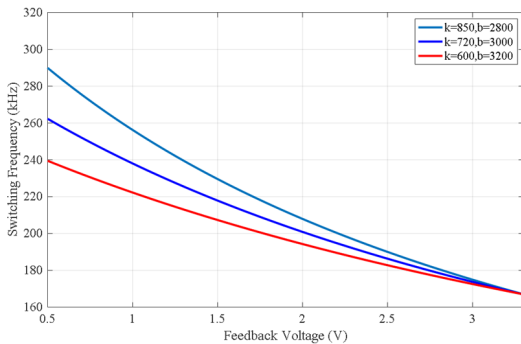


Fig. 6. Relationship between feedback voltage and switching frequency

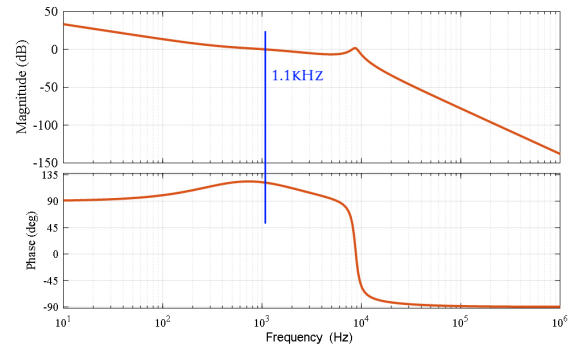
The transfer function $G_m(s)$ of the PWM generator is expressed as (12).

$$G_m(s) = \frac{df_{sw}}{dV_{fb}} = -\frac{k}{(kV_{fb} + b)^2} \frac{1}{F_n} \quad (12)$$

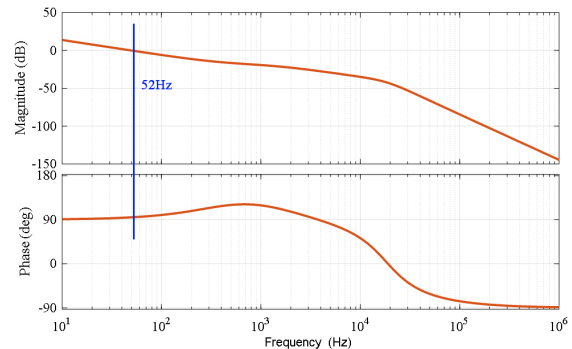
Fig. 6 shows the relationship between the feedback voltage and the switching frequency with different k and b values. From Fig. 6, the relationship between V_{fb} and f_{sw} is almost linear which means that within the feedback voltage variation range, $G_m(s)$ is constant.

To regulate the output voltage in all operating conditions and prevent the system from oscillation, the switching frequency variation step k should be designed carefully. If a small variation step is used (e.g. $k = 600$, $b = 3200$), the switching frequency range will be narrowed, and the output voltage cannot be regulated over the entire input voltage range. Conversely, if a large frequency variation step is set (e.g. $k = 850$, $b = 2800$), the switching frequency range will be increased. However, the system may become unstable, especially when the switching frequency is far away from the resonant frequency, in which the voltage gain changes faster. Thus, a compromised combination of $k = 720$ and $b = 3000$ could be a better choice by taking the switching frequency range and oscillation concern into consideration.

Fig. 7 shows the frequency responses of the open loop circuit with $k = 720$ and $b = 3000$. The crossover frequency at 250V input 1A output is 1kHz as shown in Fig. 8. But, it decreases to around 50Hz at 400V input, 40A output, which will cause slowly dynamic response.



(a) 250V input 1A output



(b) 400V input 40A output

Fig. 7. Frequency response of open loop, $R_1 = 20k\Omega$, $R_2 = 5.25k\Omega$, $R_3 = 1k\Omega$, $R_4 = 200\Omega$, $C_1 = 20nF$, $C_2 = 0.56\mu F$, and $CTR = 1.6$

III. NONLINEAR SWITCHING FREQUENCY CONTROLLER

As mentioned above, with conventional PWM generator the loop bandwidth at high input voltage reduced a lot compared to low input voltage. In theory, to obtain the best regulation performance, the switching frequency should vary slowly if the voltage gain changes quickly, and vice versa to eliminate the nonlinear characteristics. For the designed LCLC converter, the voltage gain changes along with the output current as shown in Fig. 3. It is time consuming to formulate all the opposite variations of voltage gains at different load conditions. Nevertheless, from Fig. 3 the switching frequency variations of the LCLC converter from light load to heavy load are squeezed. Therefore, one quadratic function is enough to represent the opposite variations of all voltage gain curves. Quadratic equation (13) is chosen to calculate the switching frequency.

$$\begin{aligned} T_{sw} &= \left(A_1 - A_2 (A_3 - V_{fb})^2 \right) F_n \\ f_{sw} &= \frac{1}{T_{sw}} = \frac{1}{A_1 - A_2 (A_3 - V_{fb})^2} \frac{1}{F_n} \end{aligned} \quad (13)$$

Where, A_1 , A_2 and A_3 are control parameters.

Based on (13), the gain of the PWM generator can be derived as (14).

$$G_m(s) = \frac{df_{sw}}{dV_{fb}} = - \frac{2A_2(A_3 - V_{fb})}{\left[A_1 - A_2(A_3 - V_{fb})^2 \right]^2} \frac{1}{F_n} \quad (14)$$

Fig. 8 presents the relationship between the switching frequency and the feedback voltage. As shown in Fig. 8, when the feedback voltage goes low, the switching frequency variation step goes high which will cause fast transient response at high input voltage. On the other hand, when V_{fb} goes high, the switching frequency goes low and its variation step becomes smaller, which will cause large stability margin at low input voltage. Fig. 9 shows the frequency responses of open loop circuit by using the proposed switching frequency control strategy. Particularly, at 400V input the bandwidth is increased to around 100Hz which is almost twice the bandwidth of the conventional linear method.

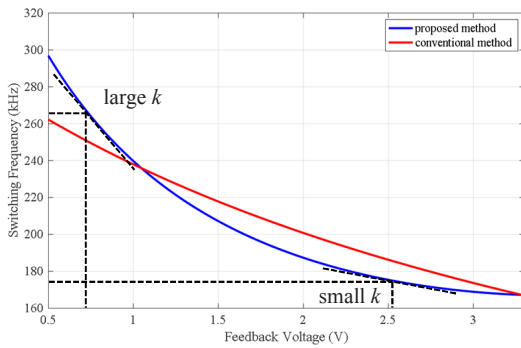
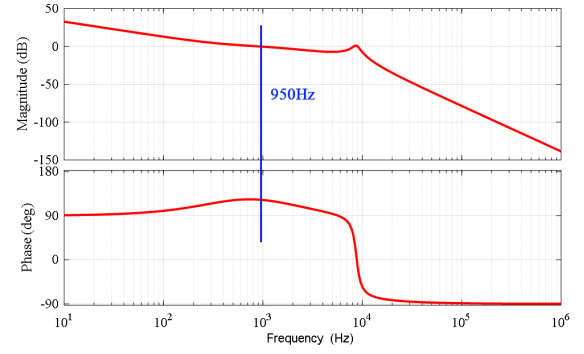
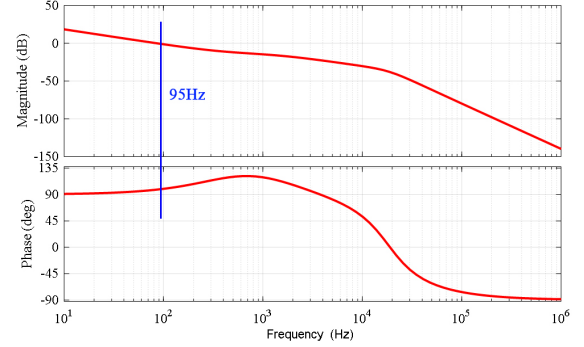


Fig. 8. Relationship between the switching frequency and feedback voltage, proposed method : $A_1 = 5600$, $A_2 = 270$, $A_3 = 3.5$; conventional method : $k = 720$, and $b = 3000$



(a) 250V input 1A output



(b) 400V input 40A output

Fig. 9. Frequency response of the open loop by using the proposed control strategy, $A_1 = 5600$, $A_2 = 270$, $A_3 = 3.5$

When the LCLC converter is built, the required switching frequency range will be fixed. Moreover, the range of the feedback voltage V_{fb} can be determined from (10) after the “TL431 + optocoupler” circuit is designed. A_1 , A_2 and A_3 are selected to ensure that f_{sw} could cover all required switching frequencies. Normally, A_1 is selected as two times of the maximum switching period value and A_3 is selected as a little bigger value than the V_{cc} , then, choosing a reasonable value for A_2 to make sure that all required switching frequencies are included.

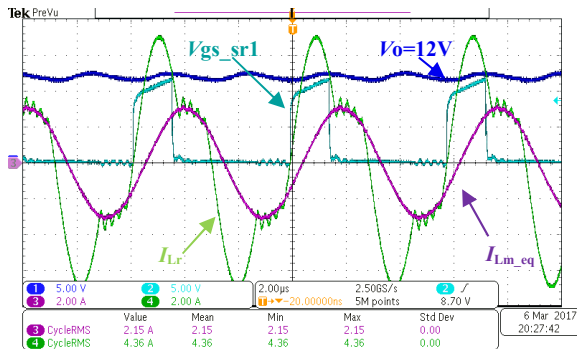
IV. SIMULATION AND EXPERIMENTAL RESULTS

To verify the effectiveness of the designed LCLC converter and the proposed nonlinear frequency controller, a 250 – 400V input 12V/500W output LCLC prototype was built and tested, as shown in Fig. 10. GaN devices (GS66516B) were used as the primary side switches. The secondary side synchronous rectifier switches were IPC100N04S5L from Infineon. Due to the limited sensing and calculation work, a low-cost MCU from Microchip is chosen in practice to perform the nonlinear switching frequency generator. To realize ZVS for primary side switches, the dead time of the PWM signals was set to 250ns. The output filter was consisted by using $9 \times 47\mu\text{F}/25\text{V}$ ceramic capacitors.

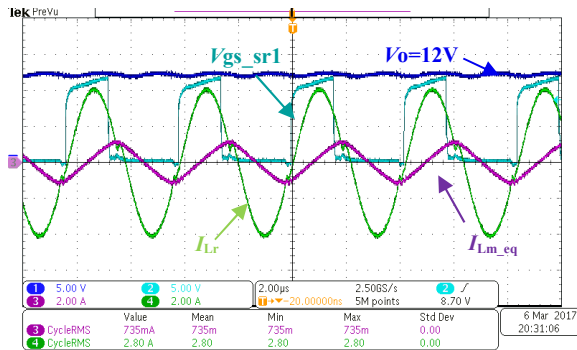
Fig. 11 presents the steady state waveforms of the LCLC converter at 250V and 400V input, 40A output, respectively. The output voltage could be regulated to 12V at both 250V and 400V input cases by using the proposed control strategy.



Fig. 10. Prototype of the 250 – 400V input 12V/500W output LCLC resonant converter



CH1: Output voltage
CH2: SR gate
CH3: Lp current
CH4: Lr current
(a) 250V input 40A output

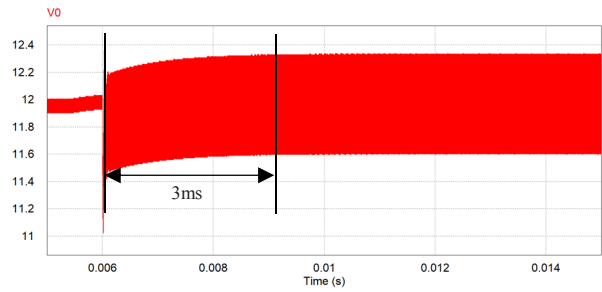


CH1: Output voltage
CH2: SR gate
CH3: Lp current
CH4: Lr current
(b) 400V input 40A output

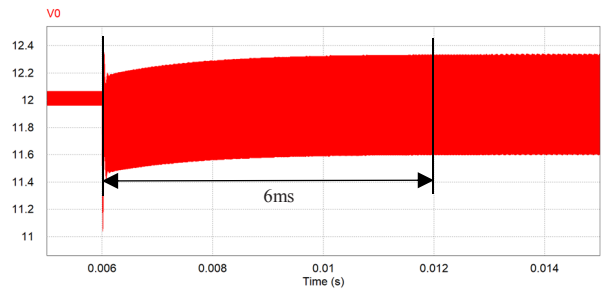
Fig. 11. Steady state waveform of the LCLC converter

Fig. 12 compares the dynamic responses of the proposed method and conventional method at 400V input using PSIM simulation. The output current experiences a sudden increase from 5A to 40A at 6ms. The setting time is 3ms for proposed control method, while 6ms for conventional method. The conventional compensator can also be designed to achieve fast dynamic response at high input voltage. But, larger switching frequency variation step k is needed, which may cause the system oscillation at low input voltage. However, by using the proposed control method, the oscillation can be effectively improved, since the switching frequency is

changing slowly at low input voltage, leading to a better performance.



(a) Proposed control method



(b) Conventional control method

Fig. 12. Dynamic responses at 400V input voltage

Fig. 13 shows the measured efficiencies of the designed LCLC converter. It demonstrates 96.8% peak efficiency and 96.4% full load efficiency at 400V input. Besides, 95% peak efficiency is achieved at 250V input, which is only 1.8% lower than that of 400V input.

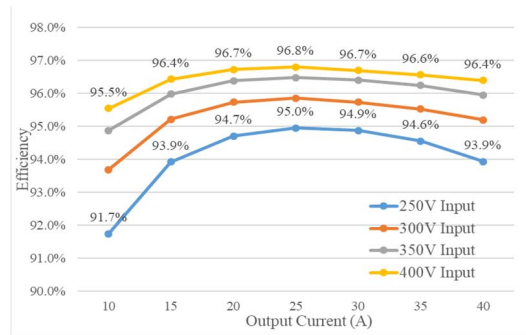


Fig. 13. Efficiencies of the developed LCLC resonant converter

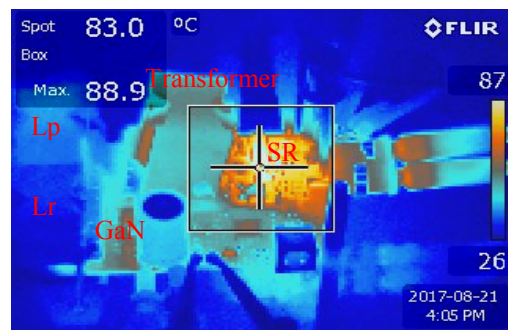


Fig. 14. Thermal image of the LCLC resonant converter

Fig. 14 shows the thermal image of the LCLC converter at 400V input, 40A output condition. The temperature of the GaN devices is 40°C. Moreover, the SRs' temperature at 400V input is around 90°C since they carry 40A current.

V. CONCLUSION

This paper proposed a nonlinear switching frequency control strategy for LCLC resonant converter to regulate output voltage at wide input voltage range. The proposed control strategy could achieve better output voltage regulation over all input voltages and improve the transient response at high input voltage. The controller is implemented by using the TL431 and optocoupler circuit plus a microcontroller. Thanks to the limited sensing and calculation assignment, a low-cost MCU was used. The details of the nonlinear switching frequency control strategy were presented. Simulation and experimental results verified the effectiveness of the proposed controller. The output voltage was regulated to its desired value over entire input voltage range. Moreover, faster dynamic response was achieved at high input voltage than that of the conventional linear method.

REFERENCES

- [1] D. Fu, B. Lu, and F. C. Lee, "1MHz high efficiency LLC resonant converters with synchronous rectifier," in *2007 IEEE Power Electronics Specialists Conference*, 2007, pp. 2404-2410.
- [2] Y. Bo, C. Rengang, and F. C. Lee, "Integrated magnetic for LLC resonant converter," in *APEC. Seventeenth Annual IEEE Applied Power Electronics Conference and Exposition (Cat. No.02CH37335)*, 2002, vol. 1, pp. 346-351.
- [3] M. D. Seeman, S. R. Bahl, D. I. Anderson, and G. A. Shah, "Advantages of GaN in a high-voltage resonant LLC converter," in *2014 IEEE Applied Power Electronics Conference and Exposition - APEC 2014*, 2014, pp. 476-483.
- [4] Y. Bo, F. C. Lee, A. J. Zhang, and H. Guisong, "LLC resonant converter for front end DC/DC conversion," in *APEC. Seventeenth Annual IEEE Applied Power Electronics Conference and Exposition (Cat. No.02CH37335)*, 2002, vol. 2, pp. 1108-1112.
- [5] A. Amirahmadi, M. Domb, and E. Persson, "High power density high efficiency wide input voltage range LLC resonant converter utilizing E-mode GaN switches," in *2017 IEEE Applied Power Electronics Conference and Exposition (APEC)*, 2017, pp. 350-354.
- [6] X. Yan, H. Lippei, C. Xuansan, and S. Stan, "A combined front end DC/DC converter," in *Applied Power Electronics Conference and Exposition, 2003. APEC '03. Eighteenth Annual IEEE*, 2003, vol. 2, pp. 1095-1099.
- [7] L. Jeong-Soo, C. Jae-Won, B. Jae-Il, O. Y. Cheol, M. Gun-Woo, and K. Chong-Eun, "Three-switch LLC resonant converter for high efficiency adapter with universal input voltage," in *2017 IEEE 3rd International Future Energy Electronics Conference and ECCE Asia (IFEEEC 2017 - ECCE Asia)*, 2017, pp. 1095-1100.
- [8] Y. Bo, X. Peng, and F. C. Lee, "Range winding for wide input range front end DC/DC converter," in *APEC 2001. Sixteenth Annual IEEE Applied Power Electronics Conference and Exposition (Cat. No.01CH37181)*, 2001, vol. 1, pp. 476-479.
- [9] B. C. Kim, K. B. Park, and G. W. Moon, "LLC resonant converter with asymmetric PWM for hold-up time," in *8th International Conference on Power Electronics - ECCE Asia*, 2011, pp. 38-43.
- [10] Y. Chen, H. Wang, Z. Hu, Y. F. Liu, J. Afsharian, and Z. A. Yang, "LCLC resonant converter for hold up mode operation," in *2015 IEEE Energy Conversion Congress and Exposition (ECCE)*, 2015, pp. 556-562.
- [11] T. Jin and K. Smedley, "Multiphase LLC series resonant converter for microprocessor voltage regulation," in *Conference Record of the 2006 IEEE Industry Applications Conference Forty-First IAS Annual Meeting*, 2006, vol. 5, pp. 2136-2143.
- [12] Z. Fang, J. Wang, S. Duan, K. Liu, and T. Cai, "Control of an LLC resonant converter using load feedback linearization," *IEEE Transactions on Power Electronics*, vol. 33, no. 1, pp. 887-898, 2018.
- [13] S. Tian, F. C. Lee, and Q. Li, "Equivalent circuit modeling of LLC resonant converter," in *2016 IEEE Applied Power Electronics Conference and Exposition (APEC)*, 2016, pp. 1608-1615.
- [14] M. Shaik and R. Kankanala, "Digital compensator design for LLC resonant converter," *Microchip Technology Inc.*, 2012.